

# **An Iterative Approach to Optimal Non-uniform Sampling and Instantaneous Bandwidth Estimation**

Nir N. Brueller, Natan Peterfreund, and Moshe Porat  
Department of Electrical Engineering, Technion, Haifa 32000, Israel

## **Abstract**

A new approach to the representation and reconstruction of non-bandlimited signals using non-uniform sampling schemes is introduced. The proposed method is based on estimation of a time-distortion transformation, under which the original signal becomes bandlimited and can thus be reconstructed. This method is optimal in the sense that it requires the minimal sampling rate for exact reconstruction of the signal. The estimation is iterative, and can be used with most available techniques of localized bandwidth approximation. An application suitable for Synthetic Aperture Radar (SAR) is given as an example. The resultant mapping can also be considered as a new means for the definition of local bandwidth.

---

Parts of this work were presented in the IEEE International Symposium on TFTS 1998, and in the IEEE International Conferences DSPA'98 and ICECS'98. This research was supported in part by the Fund for the Promotion of Research at the Technion (050-995) and by the Ollendorff Research Center.

## **Corresponding author:**

Moshe Porat  
Dept. of Electrical Engineering  
Technion Israel Institute of Technology  
Haifa 32000, Israel.  
Email: mp@ee.technion.ac.il  
Fax: +972-4-832-3041  
Tel.: +972-4-829-4684

# 1 Introduction

In a variety of applications it is desirable to represent a signal by a set of non-uniformly distributed samples [9], [12], [18]. In particular this is of interest in the case of non-bandlimited signals where an alternative approach to uniform sampling is required. In a major work on non-stationary signal representation, Clark *et al.* [5] introduced a non-uniform sampling theorem. Unlike earlier results [8], their method allows significant deviations from uniformly sampled sequences. They regarded non-uniform sampling sequences as resulting from a coordinate transformation applied to a uniformly sampled sequence. Thus the set of signals that can be exactly reconstructed from non-uniform samples can be regarded as the result of operating a time-axis distortion on a set of bandlimited signals, accordingly viewed as a transformation between a uniformly sampled bandlimited signal and an arbitrarily sampled distorted one.

Particular interest attaches to the possibility of estimating the optimal sampling instants for a non-bandlimited signal in the sense that they are transformed by the inverse time-distortion function into a uniform sampling sequence of a bandlimited signal. This permits error-free reconstruction, provided the sampling rate on the distorted grid satisfies the Nyquist condition. Application of the distortion function then enables the original signal to be reconstructed. The relation between the time-distortion function and the instantaneous frequency as shown by Poletti in [10], motivates our approach. For example, the Wigner-Ville distribution whose kernel is unity has a mean conditional frequency that equals the derivative of the time-distortion function.

The Fourier transform of a signal takes into account its spectral components at all times. It is therefore obvious that sampling non-stationary signals at their global Nyquist rate is not cost-effective as far as the sampling rate is concerned. In most signals, there are regions where the bandwidth is narrower, and accommodates a lower sampling rate. Knowledge of the signal's instantaneous bandwidth would ideally make it possible to transform it into a bandlimited signal. In the absence of an exact local bandwidth measure, however, we employ a new iterative process in realizing the required time-distortion transformation. The fact that the results of this iterative process are independent of the Time-Frequency Distribution (TFD) used at each stage, indicates that the resulting time-distortion transformation can be regarded as a robust measure of the signal, defining local bandwidth.

This paper is organized as follows. Section 2 describes non-uniform sampling and shows the relation between the time-distortion function and the instantaneous bandwidth. Section 3 proposes an iterative method for non-uniform sampling and reconstruction of non-bandlimited signals. Section 4 deals with error analysis, Section 5 provides numerical examples and Section 6 presents an application suitable for Synthetic Aperture Radar (SAR). Concluding remarks are summarized in Section 7.

## 2 Non uniform sampling

Based on the time axis transformation approach, we introduce a new algorithm for sampling and reconstruction of signals from a set of non-uniform samples. In our algorithm we use a theorem [5], which states that if a signal  $f(t)$  is sampled at  $t=t_n$  (not necessarily uniformly spaced) and if a one-to-one continuous mapping function  $\gamma(t)$  exists such that  $\gamma(t_n)=nT$  and  $f(\gamma^{-1}(\tau))$  is bandlimited to  $\omega_0=\pi/T$ , then

$$f(t) = \sum_{n=-\infty}^{\infty} f(t_n) \text{sinc}[\omega_0(\gamma(t) - nT)]. \quad (1)$$

We consider this approach to be optimal in the sense that it requires the minimal sampling rate for error-free reconstruction of non-bandlimited signals. Clark *et al.* [5] showed also that their approach is analogous to Horiuchi's reconstruction [7], and argued that the derivative of this mapping, or distortion transformation, can be considered as instantaneous bandwidth:

$$\frac{\partial \gamma(t)}{\partial t} = \frac{2\pi}{\omega_0} B(t) \quad ; \quad \gamma(t) = \int_0^t \frac{2\pi}{\omega_0} B(r) dr . \quad (2)$$

The above theorem requires knowledge of  $\gamma(t)$  for every  $t$ , in addition to all the sampling instants  $t_n$  and their associated samples  $f(t_n)$ . Unless we have an analytic expression for  $\gamma(t)$ , this function must be estimated, for example by means of interpolation with the constraint of a one-to-one and invertible  $\gamma(t)$  [5]. The major difficulty in applying this method to an arbitrary given signal is the evaluation of the required time-distortion transformation  $\gamma(t)$ . The fact that the latter requires integration over the instantaneous bandwidth (2) suggests that it could be approximated on the basis of instantaneous bandwidth estimates. A special case of interest, that demonstrates the relation in (2) between the local bandwidth and the distortion transformation is the frequency modulated signal:

$$s(t) = a(t) e^{j\phi(t)} . \quad (3)$$

The instantaneous bandwidth equals in this case to the instantaneous frequency, which was shown by Poletti [10] to be estimated error-free using the conditional frequency of the Wigner-Ville distribution:

$$\langle \omega | t \rangle = \phi'(t) . \quad (4)$$

This result is the motivation for using the local bandwidth estimation as a means for estimating the time-distortion function of a given signal. In the case of arbitrary signals which do not belong to the above form, one can use time-frequency transformations for evaluating the instantaneous (local) bandwidth. The local bandwidth of a signal is defined as follows:

**Definition:** Given a time frequency distribution  $F(\omega, t)$  of a signal  $f(t)$ , the local bandwidth at time  $t$  is defined as the maximal  $\omega$  with 3dB deviation with respect to  $\max_{\omega}\{F(\omega, t)\}$ .

An example for time-frequency transformation, which could be used to estimate the local bandwidth, is the practical form of the windowed Wigner-Ville distribution defined by:

$$W_x(t, f) = \int_{-T}^T x\left(t + \frac{\tau}{2}\right) x^*\left(t - \frac{\tau}{2}\right) w\left(\frac{\tau}{2}\right) w^*\left(-\frac{\tau}{2}\right) e^{-j2\pi f\tau} d\tau, \quad (5)$$

where:

$$w(t) = 0 \quad \text{for} \quad |t| > \frac{T}{2}. \quad (6)$$

An efficient real-time implementation of the Wigner-Ville distribution was offered by Boashash [3]. The Short Time Fourier Transform (STFT), calculated by realizing the Fourier transform on the windowed signal:

$$X_w(t, f) = \int_{t-\frac{T}{2}}^{t+\frac{T}{2}} x(\tau) w(\tau - t) e^{-j2\pi f\tau} d\tau, \quad (7)$$

$w(t)$  being a window function such that:

$$w(\tau) = 0 \quad \text{for} \quad |\tau| > \frac{T}{2}, \quad (8)$$

also showed good results in estimating the local bandwidth. Its drawback lies in the inverse relation between the time and frequency resolutions. Extension of the window's length improves the frequency resolution but deteriorates the temporal selectivity.

There are many other possible techniques for estimating local bandwidth (e.g., [6]), most of which suffer from limited accuracy. This aspect is further elaborated in the following section.

### 3 Time-distortion transformation

The time-distortion transformation is calculated by (2) using the instantaneous bandwidth estimate. In order to remedy the limited accuracy of the time-frequency distribution in estimating the local bandwidth, an iterative approach is proposed, under which the distortion function is realized in an accumulative

manner, each iteration being aimed at compensating for the differences in the instantaneous bandwidth remaining after the previous iteration. It is important that each iteration, though not having translated the signal immediately to a constant bandwidth signal over the distorted axis, would in general make the bandwidth over the inversely distorted axis more uniform. This process converges and reaches a stage where the signal acquires a constant instantaneous bandwidth over the distorted time axis.

The suggested iterative process is as follows. The local bandwidth  $B(t)$  of the signal is estimated by means of a windowed transform. This estimate  $\hat{B}(t)$  is then integrated over time, as presented in (2), yielding an estimate of the distortion function  $\hat{\gamma}(t)$ . At that stage a function  $\hat{\alpha}(t)$  has to be found, to serve as the inverse operation of the estimated  $\hat{\gamma}(t)$ , or, in other words, to undo the distortion caused by  $\gamma(t)$ , such that the following relation holds:

$$\gamma(\hat{\alpha}(t)) \approx t. \quad (9)$$

The function  $\hat{\alpha}(t)$  transforms *chronological* time into *weighted* time, meaning that the time instant associated with each point of the given signal will depend on the original time instant of that point and on the local instantaneous bandwidth estimate,  $\hat{B}(t)$ , over the duration of the examined signal  $[0, t_{\max}]$ .

This approach could also be interpreted as *scaling* in the following context. It is well known that by scaling a signal in the time domain we achieve inverse scaling of its Fourier transform in the frequency domain, i.e.,

$$\mathbf{F}\{f(t)\} = F(\omega) \Rightarrow \mathbf{F}\{f(at)\} = \frac{1}{|a|} F\left(\frac{\omega}{a}\right). \quad (10)$$

Using (10), we propose an alternative approach to inverse transformation of the time axis by  $\gamma^{-1}(t)$ . As will be shown, although this method is less accurate per iteration, it achieves faster and better results.

We try to distort the time axis so that the signal acquires constant instantaneous bandwidth. To this end, we perform an *instantaneous* scaling operation on the signal in the time domain. The scaled time axis is then given by:

$$\hat{t} \equiv \alpha(t) = \frac{\int_0^t \frac{1}{\hat{B}(r)} dr}{\int_0^{t_{\max}} \frac{1}{\hat{B}(r)} dr} t_{\max}. \quad (11)$$

Such a mapping makes  $\hat{t}$  progress faster in regions of relatively narrow bandwidth, and slower in regions of higher bandwidth. The time axis of a constant local bandwidth signal would be mapped onto itself, meaning that it would remain invariant while this algorithm is implemented. The stages of the iterative process are shown in Figure 1.

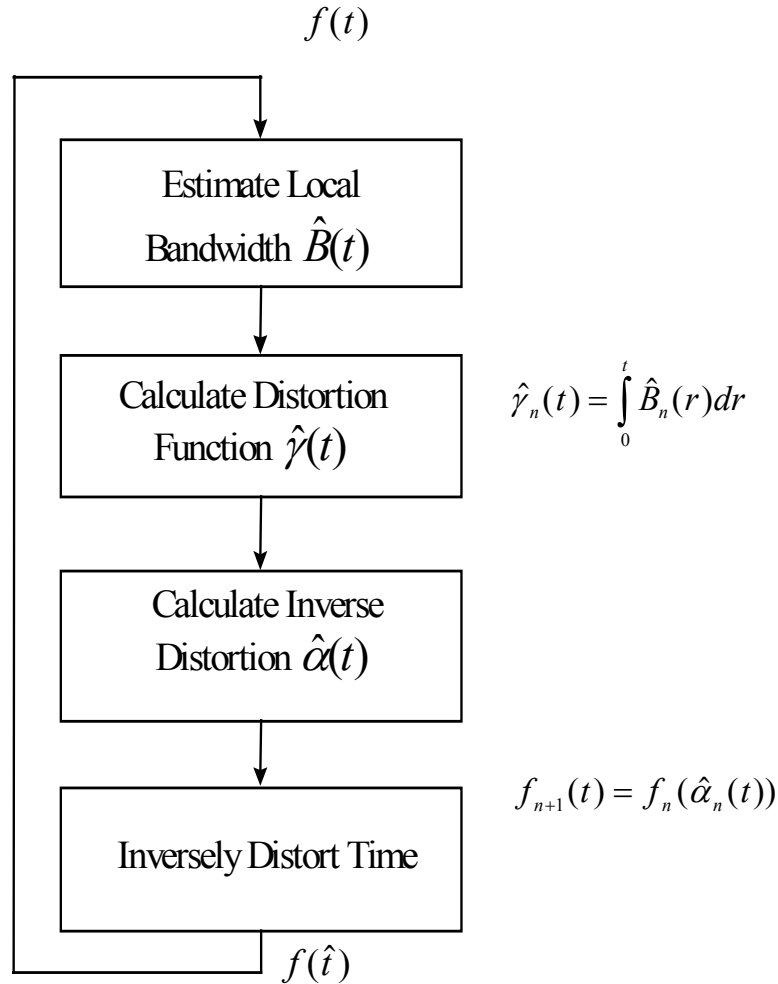


**Figure 1 - Flowchart of the iterative algorithm.  $n$  indicates the iteration number.**

Let  $B_n(t)$ ,  $\hat{B}_n(t)$ ,  $\hat{e}_n(t)$  denote the instantaneous bandwidth, estimated instantaneous bandwidth and estimation error in the  $n$ -th iteration respectively, such that:

$$\hat{B}_n(t) = B_n(t) + \hat{e}_n(t). \quad (12)$$

Substituting  $\hat{\alpha}(t)$  in  $f(t)$  results in a new signal, whose bandwidth changes more slowly than that of the original:

$$B_n(t) = \frac{\partial \gamma_{n-1}(\hat{\alpha}(t))}{\partial t} = \frac{B_{n-1}(\hat{\alpha}(t))}{\hat{B}_{n-1}(t) \left\langle \frac{1}{\hat{B}_{n-1}} \right\rangle}, \quad (13)$$

where:

$$\left\langle \frac{1}{\hat{B}} \right\rangle = \frac{\int_0^{t_{max}} \frac{1}{\hat{B}(t)} dt}{t_{max}}. \quad (14)$$

It can be seen that when the bandwidth estimation is error-free and constant, it will remain unchanged. Otherwise we iterate this algorithm until we reach the point where  $\gamma_n \approx \alpha_n(t) \approx t$ . The function  $\gamma(t)$  is then reconstructed from:

$$\hat{\gamma}_1(\hat{\gamma}_2(\dots \hat{\gamma}_{n-1}(\hat{\gamma}_n(t)) \dots)) \cong \gamma(t), \quad (15)$$

where  $n$  denotes the iteration number. The accuracy of this iterative approximation of  $\gamma(t)$  improves as the number of iterations increases and is shown to converge.

It should be noted that although using  $\hat{\gamma}^{-1}(t)$  instead of  $\hat{\alpha}(t)$  may seem as an intuitive alternative, it reduces the convergence rate and requires more calculations (of  $\hat{\gamma}(t)$ , then interpolation to calculate  $\hat{\gamma}^{-1}(t)$ ).

## 4 Error Analysis

The above methods for bandwidth estimation require that the signal be stationary over the estimation interval (while the window function is non-zero). Poletti [10] suggests local expansion of the signal for analyzing its change of phase. The first derivative of the phase indicates linear change, and for assessing the non-linearity of the phase, its second derivative has to be considered. Rihaczek has previously proposed such a definition in [14], representing the relaxation time of a signal of the form:

$$s(t) = a(t) e^{j\phi(t)}. \quad (16)$$

Considering the first and second derivatives of the phase, and ignoring the temporal change in signal magnitude, we get:

$$s(t + \tau) = a(t + \tau) e^{j\phi(t+\tau)} \approx a(t) e^{j\phi(t)} e^{j\left[\phi'(t)\tau + \frac{\phi''(t)}{2}\tau^2\right]}. \quad (17)$$

Rihaczek defined the relaxation time as the period in which the phase deviation from its linear model does not exceed  $\pi/4$ . The window length to be used for local bandwidth estimation of the signal should therefore not exceed:

$$T_r = \sqrt{\frac{2\pi}{|\phi''(t)|}}. \quad (18)$$

The instantaneous relaxation bandwidth would then become:

$$\sigma_r^2 = \frac{|\phi''(t)|}{2\pi}. \quad (19)$$

This analysis is not always valid in our case. Since we often view a signal using a window longer than its relaxation time, the resulting error must be taken into account.

Analysis of the spectral description of an LFM (Linear Frequency Modulation) waveform clearly shows that the half-power cutoff expresses the frequency range observed during the window [15]. As an example, the instantaneous local bandwidth (instantaneous frequency) of three chirp LFM signals with different slopes is given in Figure 2.

$$\begin{aligned} f_1(t) &= \sin(0.3t^2) \\ f_2(t) &= \sin(0.6t^2) \\ f_3(t) &= \sin(0.9t^2) \end{aligned} \quad (20)$$

The Fourier transforms of these three signals are shown in Figure 3.

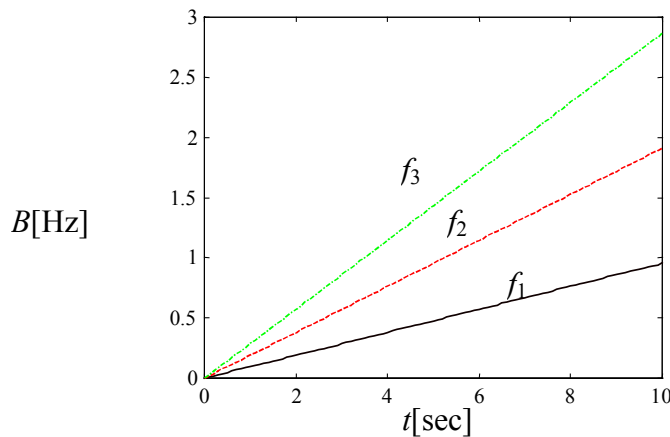
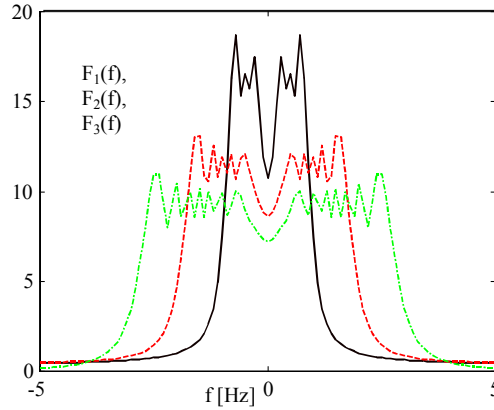


Figure 2 - Local Bandwidth (instantaneous frequency) for three different LFM signals.



**Figure 3 - The Fourier transform of the three LFM signals of Figure 2.**

This justifies assumption of a model for the local bandwidth estimation error. The latter is random, but could be approximated using the derivative of the instantaneous bandwidth:

$$e = |B'| \frac{T}{2} (1+r), \quad (21)$$

where  $r$  is a random variable, uniformly distributed in the interval

$$-0.5 < r < +0.5. \quad (22)$$

The error is in fact included in our bandwidth measurements:

$$\hat{B}_n(t) = B_n(t) + e(t). \quad (23)$$

The results of the Monte-Carlo estimation given in Figure 4 show the maximum standard deviation of all signal points, where the original signal is:

$$x(t) = \sin(0.8 \cdot t^2). \quad (24)$$

In order to assess how errors in the bandwidth estimation affect the convergence of the iterative process, we have simulated the bandwidth change between iterations using (13), adding noise (21) to the bandwidth estimation. This method allows to assess the influence of the bandwidth estimation error on the convergence of the iterative process.

The convergence of the process is demonstrated in Figure 4.

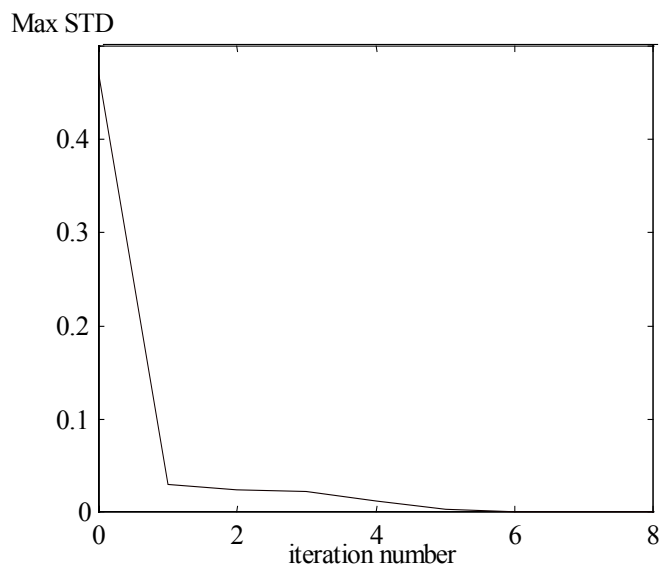


**Figure 4 - Results of a Monte-Carlo estimation.**

The convergence of the iterative process was also tested for noisy signals. Uniform noise at various intensities was added to the original signal, then the iterative process was performed. The results are shown in Figure 5, indicating immunity to noise for SNR greater than 18dB.

The different results for the noise-free case between Figure 4 and Figure 5 are due to the fact that Figure 4 shows simulated results as described above, while Figure 5 shows results where all the stages of the iterative process have been performed.

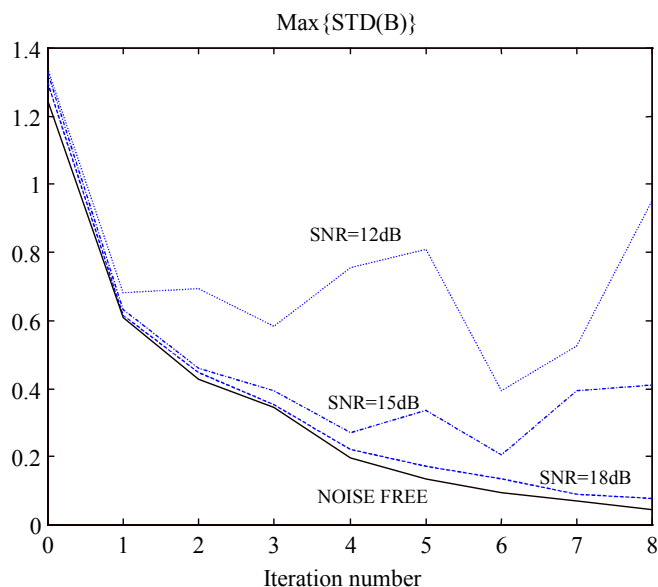


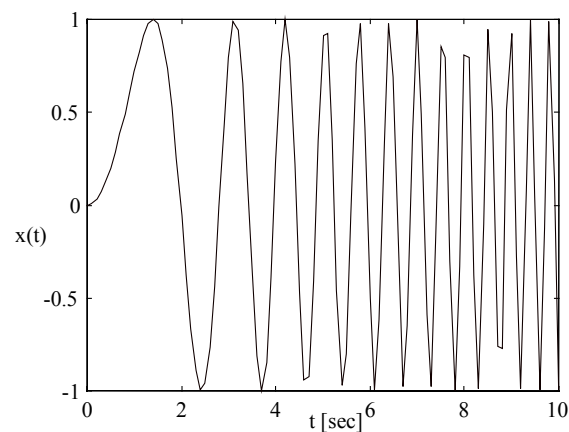
**Figure 5 - Convergence of the iterative process - maximal standard deviation for uniformly distributed noise with SNR of 12dB, 15dB and 18dB, compared to the noise-free case (solid).**

## 5 Numerical Examples

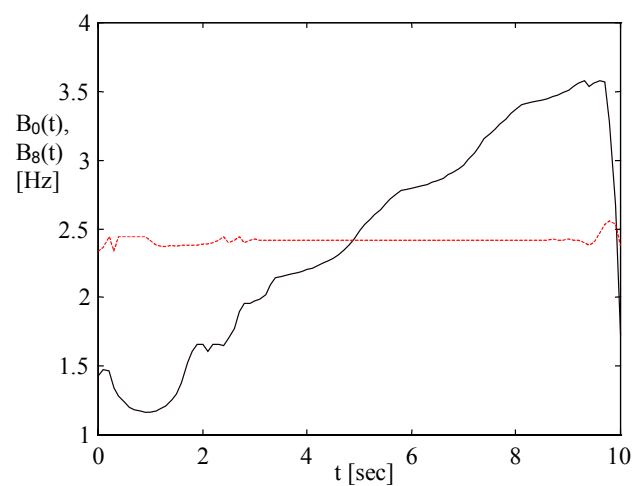
Three signals are considered in this section as examples.

### 5.1 Example #1

The first example is the FM signal of equation (24), presented in Figure 6. The signal consists of 100 equally spaced samples and its instantaneous spectral content is estimated by means of STFT (Figure 7, solid line).



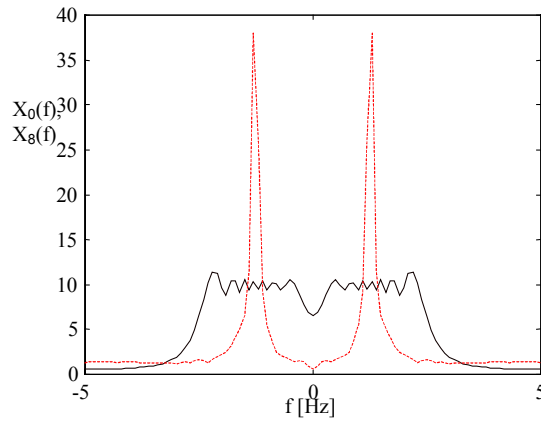
**Figure 6 - The signal in the time domain.**



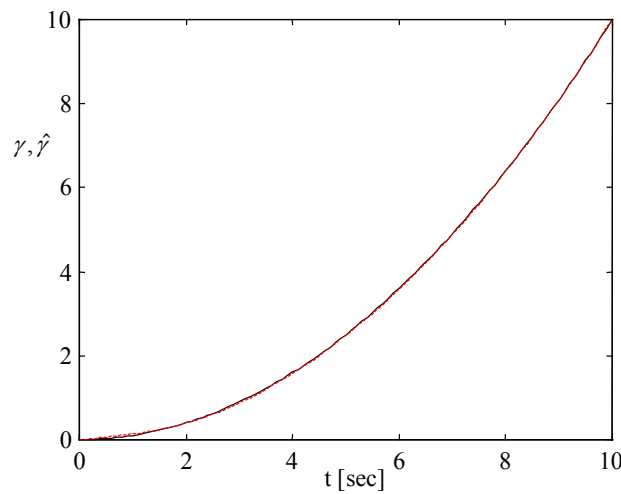
**Figure 7 - Instantaneous bandwidth estimates at the beginning (solid) and the end (dashed) of the process.**

Figure 7 also shows the local bandwidth after eight iterations (dashed), where it varies significantly less than at the beginning of the process. In Figure 8 the Fourier transforms of the entire signal at the beginning and the end of the process are presented

Figure 9 shows the original time-distortion function, and the one found by the iterative analysis after eight iterations. As can be seen, the proposed iterative process accurately estimates the time-distortion function.



**Figure 8 - Fourier transform of the signal at the beginning (solid) and the end (dashed) of the process.**



**Figure 9 - The time distortion function - theoretical value (original gamma, solid) and its estimate (dashed).**

Figure 9 shows the Time-Frequency (TF) distribution of the original signal using STFT. The linear change of the instantaneous frequency is clearly seen. Figure 10 shows the TF representation at the end of the process, with the instantaneous frequency practically constant.

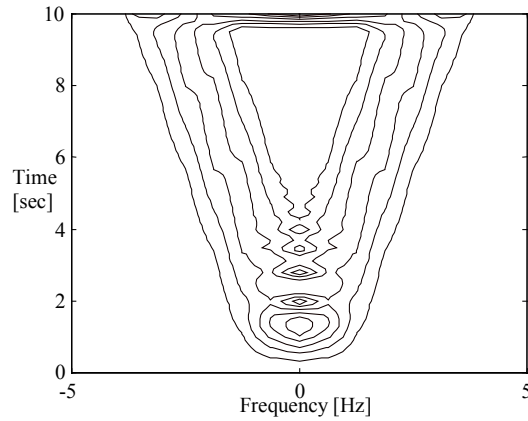


**Figure 10 - Time-Frequency representation of the original signal (STFT).**

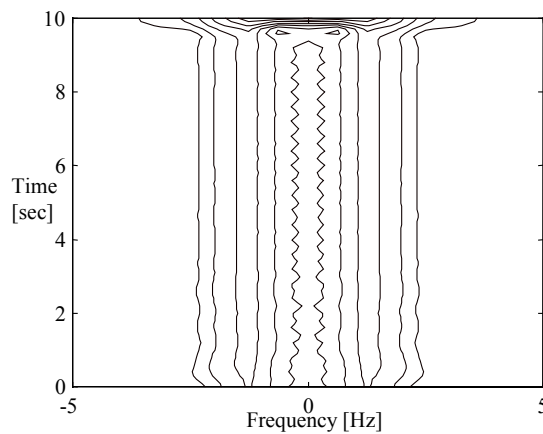


**Figure 11 - Time-Frequency representation of the final signal (STFT).**

The average difference (over all the points in time) between the original  $\gamma$  and the approximated  $\hat{\gamma}$  was calculated after each iteration and the results are presented in Figure 12. Figure 13 compares the original and the reconstructed signals.

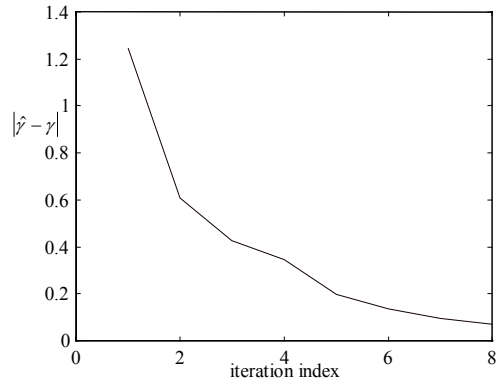


**Figure 12 - The average difference between the original  $\gamma$  and the approximated  $\hat{\gamma}$ .**

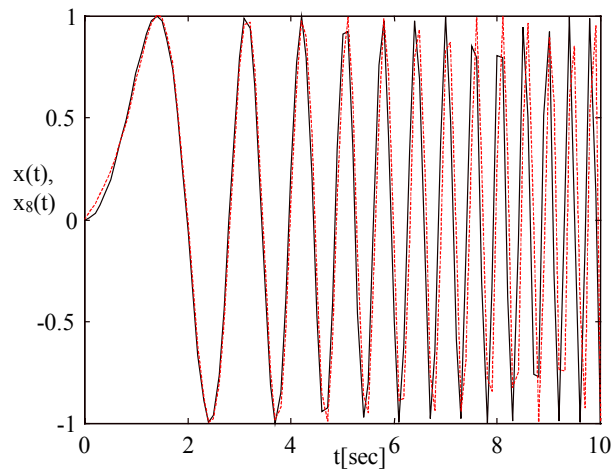


**Figure 13 - Original (solid) and reconstructed signal (dashed).**

## 5.2 Example #2

The second example deals with a sine-wave, presented in Figure 14:

$$x(t) = \begin{cases} \sin(2\pi t) & t \in [0,5] \\ \sin(3\pi t) & t \in (5,10] \end{cases} \quad (25)$$

This signal again consists of 100 equally time spaced samples and, as shown in Figures 15, the resulting signal after eight iterations (dashed), has an almost constant local bandwidth. Figure 16 compares the original and the reconstructed signals.

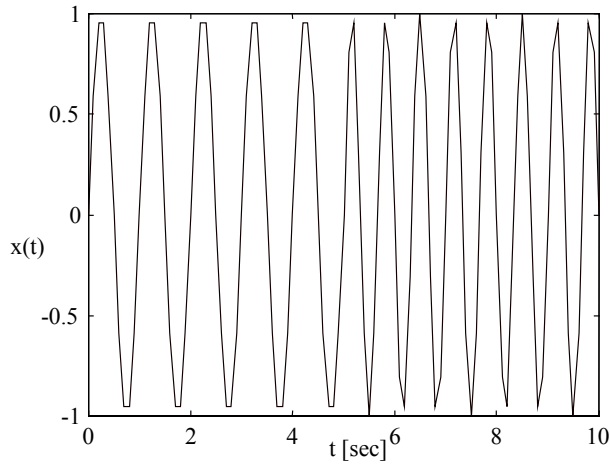


**Figure 14 - The signal in the time domain (second example).**

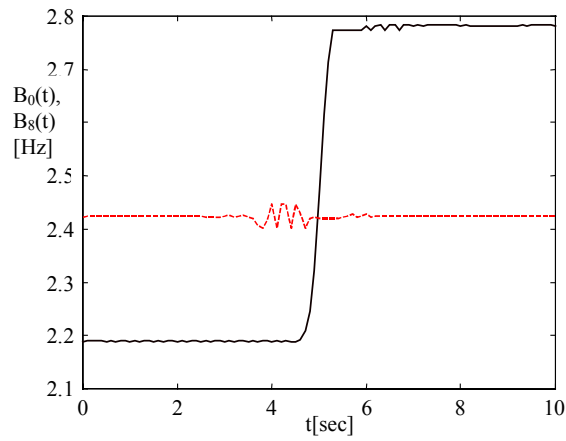


**Figure 15 - Instantaneous bandwidth estimates at the beginning (solid) and the end (dashed) of the process for the second example.**

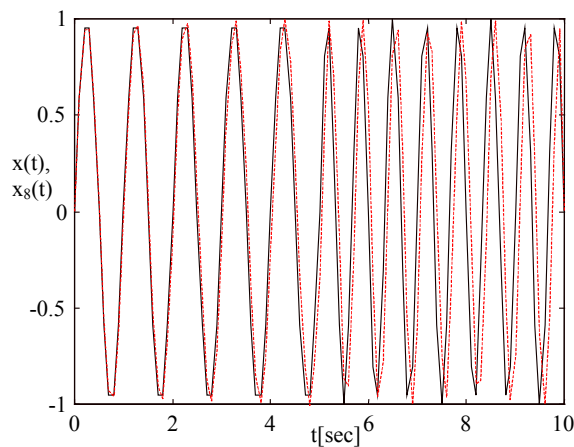


**Figure 16 - Original (solid) and reconstructed signal.**

### 5.3 Example #3

The last example is of an audio signal. As can be concluded, the proposed method is capable of analyzing, presenting and reconstructing also a natural signal, similar to the results obtained for the synthetic examples (Figures 17, 18 and 19).

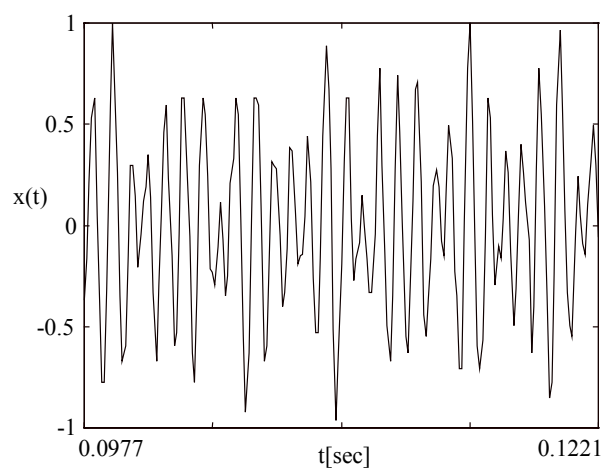


**Figure 17 - The signal in the time domain (audio signal).**

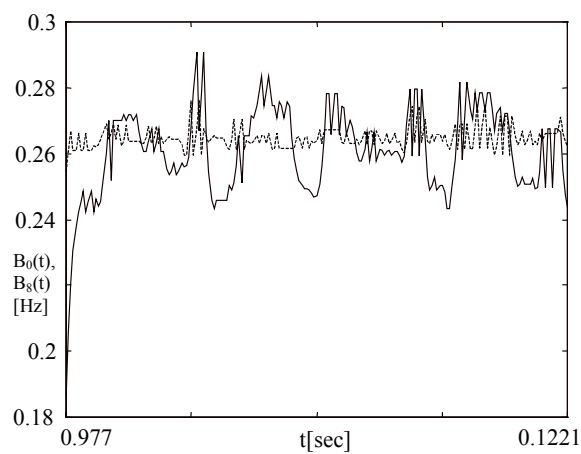


**Figure 18 - Initial (solid) and final (dashed) instantaneous bandwidth of the audio signal.**

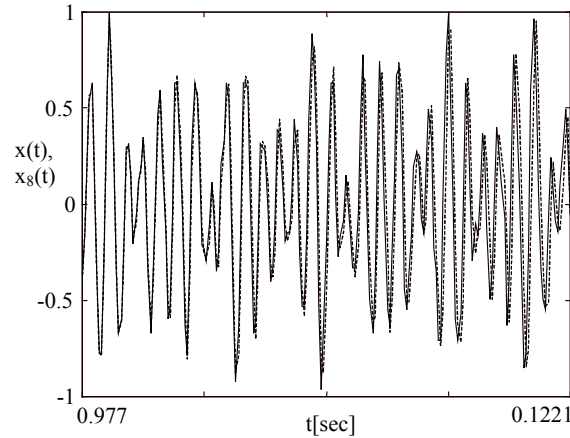


**Figure 19 – Original (solid) and reconstructed audio signal (dashed).**

## 6 Application - Synthetic Aperture Radar

The Synthetic Aperture Radar (SAR) [4] has been used extensively recently to generate long synthetic antennas based on the radar's motion. This antenna can be used for high-resolution imagery of the terrain. High resolution in the range direction is usually achieved by compressing a wide-band pulse, whereas the high resolution in the azimuth direction is achieved due to coherent processing of the radar returns received along a certain flight path (synthetic aperture).

The SAR algorithm can be interpreted as a two-dimensional matched filter that allows the compression both in range and azimuth of the radar returns from a static point scatterer. Any deviation from the ideal scenario, in which the platform's position is perfectly known and all the ground scatterers are static, degrades the quality of the obtained image.

In practice, platforms do not move along straight lines, and the Inertial Measuring Units (IMU), installed on board, cannot properly compensate for the errors in the platform's location. These residual errors can be corrected according to the received data itself. Based on the Phase History of a dominant scatterer, which is assumed to be static, it is possible to correct the phase of the entire image, a process called *Auto Focus*. In the next paragraph we will demonstrate this processing using the iterative algorithm shown earlier in this work.

In a typical Spot Light SAR scenario the radar antenna continuously illuminates the same area on the ground (spot). The geometry and the required processing aperture are given based on [16].

Consider the transmitted signal

$$S_t(t) = e^{-j\left(\omega t + \pi \frac{B}{t_p} t^2\right)}, \quad (26)$$

where  $B$  is the LFM (Linear Frequency Modulation) bandwidth and  $t_p$  the width of the transmitted pulse.

This signal is back-scattered from points  $m,n$  with reflectivity  $A_{m,n}$ . The overall returned signal is calculated based on the contributions of all the back-scattering elements:

$$S_r(t) = \sum_{m,n} A_{m,n} e^{-j\left[\omega\left(t - \frac{2\bar{R}_{m,n}}{c}\right) + \pi \frac{B}{t_p} \left(t - \frac{2\bar{R}_{m,n}}{c}\right)^2\right]} \quad (27)$$

where  $\frac{2\bar{R}_{m,n}}{c}$  is the time delay between the transmitted and received signals, which corresponds to the range  $\bar{R}_{m,n}$ .

The platform's range from the center of the spot in the azimuth axis in the  $m$ -th range cell is

$$R_{m,n}(t) = \sqrt{x_{m,n}^2 + (y_0 - vt)^2 + z^2} \quad (28)$$

where  $z$  is the altitude of the radar.

The range definition can be expanded for different cells in the azimuth axis:

$$\bar{R}_{m,n}(t) = \sqrt{x_{m,n}^2 + (y_0 - vt - \Delta y_{m,n})^2 + z^2}. \quad (29)$$

Assuming that  $\Delta y_{m,n} \ll R_{m,n}(t)$  we get:

$$\bar{R}_{m,n}(t) \cong R_{m,n}(t) - \frac{(y_0 - vt)\Delta y_{m,n}}{R_{m,n}(t)} + \frac{\Delta y_{m,n}^2}{2R_{m,n}(t)}. \quad (30)$$

The geometric configuration is presented in Figure 20.

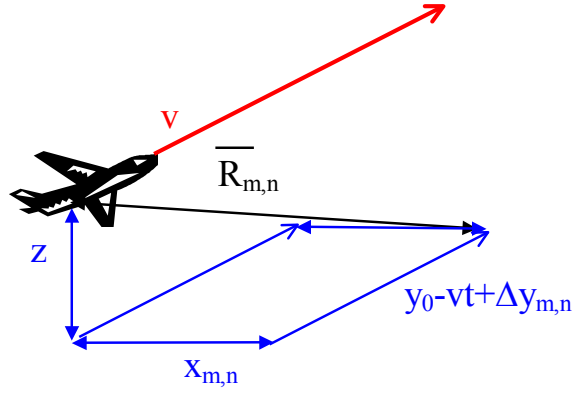


Figure 20 - Typical SAR imaging geometry.

In processing the received information in Spot Light SAR, it is suitable to use the a dechirping process. This can be mathematically described in the following manner [16]:

$$S_t(t) \cdot S_r^*(t + \tau) = \sum_{m,n} A_{m,n} e^{j(f_{m,n} + F_{m,n})} \quad (31)$$

where  $f_{m,n}$  is a component generated by the Doppler effect and is used to determine the azimuth of the scatterer:

$$f_{m,n} = \frac{2kvt\Delta y_{m,n}}{R_{m,n}}; \quad k = \frac{\omega}{c}. \quad (32)$$

$F_{m,n}$  contains two components; the first is linear in time (part of the chirped signal) and is used for range measurement. The second is a constant phase element, the residual videophase, quadratically dependent on the difference from the center of the spot, and may be neglected if the spot is small.  $F_{m,n}$  is described by:

$$F_{m,n} = \pi \frac{B}{t_p} \left[ 2t \left( \tau - \frac{2R_{m,n}}{c} \right) + \left( \tau - \frac{2R_{m,n}}{c} \right)^2 \right]. \quad (33)$$

The first additive term is the argument of a sine-wave whose frequency corresponds to the difference between the range to the point  $R_{m,n}$  and the range to the center of the spot. This process limits the possible spot-size due to the requirement for simultaneous existence of the received signal and the reference signal over a period of time long enough to achieve the required resolution even at the edges of the spot. Range determination is performed by means of the Fourier transform of (32).

This focusing method is usually based on one prominent reflector. Analyzing the phase history of this reflector allows retrieving the information describing the deviations that have occurred in the flight path and then use this information to compensate for such deviations. This process of Auto-focus is based on the data itself.

For simplicity we will chose  $y_0, \Delta y_{m,n} = 0$ , and therefore  $R = \sqrt{x^2 + z^2}$ .

The time dependent range can be defined as

$$R(t) = \sqrt{R^2 + v^2 t^2} = R \sqrt{1 + \frac{v^2 t^2}{R^2}} \cong R + \frac{v^2 t^2}{2R} ; vt \ll R. \quad (34)$$

The range between the radar and the mapped area can increase or decrease, depending on the squint angle (forward or backwards).

The Phase history due to the target's motion is therefore:

$$\phi(t) = \frac{4\pi}{\lambda} R(t) \cong \frac{4\pi}{\lambda} \left( R + \frac{v^2 t^2}{2R} \right), \quad (35)$$

and after compensating for the motion as measured by the IMU, the remainig error usually stems from the sweeping accelaration  $\varepsilon$ :

$$s(t) = e^{j(2\pi f_D t + \varepsilon t^2)}. \quad (36)$$

Using typical numbers for example, we get:

$$s(t) = e^{j(50t + 3t^2)}, \quad (37)$$

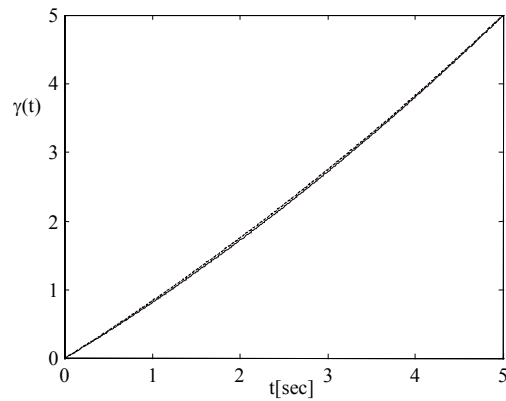
and the remaining time-distortion function is therefore:

$$\gamma = 50t + 3t^2. \quad (38)$$

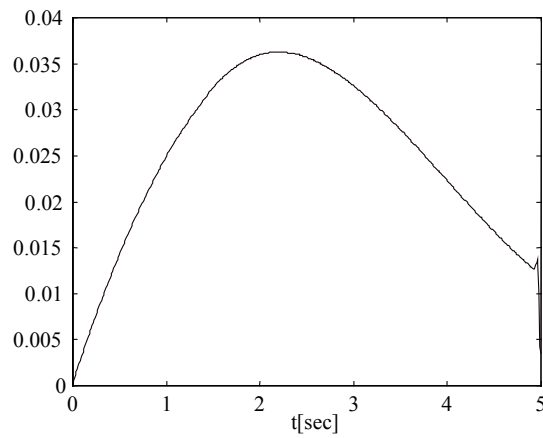
This time-distortion function is given in Figure 21 along with the its estimation, based on 8 iterations of the iterative process.

Figure 22 shows the reconstruction error, indicating the difference between the original time-distortion function and its reconstruction.

Figure 23 shows the impulse response before and after performing autofocusing. This impulse response also represents the resolution achieved in the azimuth axis.



**Figures 21 – Time-distortion function - theoretical (solid) and estimated (dashed).**



**Figure 22 -  $\gamma$  estimation error.**

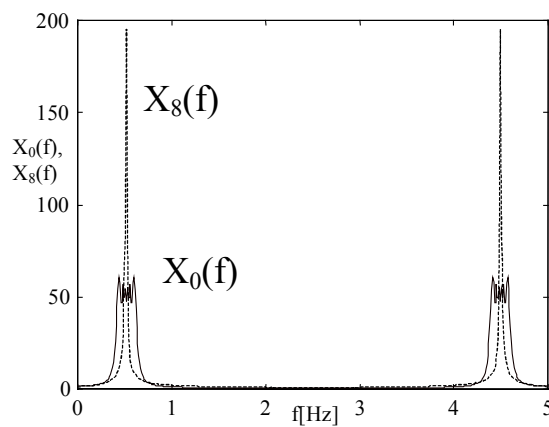


**Figure 23 - Initial (solid) and final (dashed) Fourier transforms express the impulse response that shows the resolution achieved.**

Assume that the static reflector  $m,n$  is replaced by a moving reflector with velocity  $v_{m,n}$ . Its position in time is given by:

$$\Delta y_{m,n}(t) = \Delta y_{m,n} + v_{m,n}t, \quad (39)$$

Thus the generalized Doppler term becomes

$$G(\tau) = S_i(t) \cdot S_r^*(t + \tau) \approx \sum_{m,n} A_{m,n} e^{j \left( \frac{2kv_0 t \Delta y_{m,n}}{R_{m,n}} + \frac{2kv_0 v_{m,n} t^2}{R_{m,n}} \right)}. \quad (40)$$

Analysis of this signal can be performed using a TFD (Time-Frequency Distribution), as demonstrated in [1], [2], [13] and [16]. Unlike the Fourier Transform, however, such a transformation allows presentation of non-stationary signals as well. Performing the iterative process on such a signal enables to compensate for the phase variation witnessed by a moving target, hence allowing its mapping using SAR.

## 7 Concluding Remarks

A new approach to optimal representation and reconstruction of non-stationary signals has been introduced. This iterative approach which can be based on various approximations of bandwidth estimate, converges to a consistent definition of local bandwidth irrespective of the specific technique used. According to this definition, a transformed version of the signal can be represented and reconstructed from a set of non-uniformly spaced samples of the signal, thus providing an efficient means for non-stationary signal storage and processing. It has been found and shown that the proposed estimation is robust and efficient both in implementation and in the number of iterations required for practical convergence.

Based on our results, it is concluded that the new approach can provide an efficient solution to representation of signals as introduced and discussed in the basic studies of Horiuchi [7] and Clark *et al.* [5], making their observations of practical use. An example of SAR imaging has been described and considered in this context, illustrating the capability of the proposed algorithm. Such applications could serve in the efficient representation of nonstationary signals, where further research in the coding of the distortion function  $\gamma$  could be instrumental for compression purposes [18] and signal representation by partial information [11], [17].

## References

- [1] S. Barbarosa, "Detection and Imaging of Moving Targets with Synthetic Aperture Radar, Part 1: Optimal Detection and Parameter Estimation Theory", *IEE Proceedings-F*, Vol. 139, No. 1, pp. 79-88, 1992.
- [2] S. Barbarosa and A. Farina, "Detection and Imaging of Moving Targets with Synthetic Aperture Radar, Part 2: Joint Time-Frequency Analysis by Wigner-Ville Distribution", *IEE Proceedings-F*, Vol. 139, No. 1., pp. 89-97, 1992.
- [3] B. Boashash and P. J. Black, "An Efficient Real-Time Implementation of the Wigner-Ville Distribution", *IEEE Transactions on Acoustics, Speech and Signal Processing*, Vol. ASSP-35, No. 11, 1987.
- [4] W. G. Carrara, R. S. Goodman and R. M. Majewski, "Spotlight Synthetic Aperture Radar: Signal Processing Algorithms", Artech House, 1995.
- [5] J. J. Clark, M. R. Palmer and P. D. Lawrence, "A Transformation Method for the Reconstruction of Functions from Non-uniformly Spaced Samples", *IEEE Transactions on Acoustics, Speech and Signal Processing*, Vol. ASSP-33, No. 4, pp. 1151-1165, 1985.
- [6] A. Francos and M. Porat, "Analysis and Synthesis of Multicomponent Signals using Positive Time-Frequency Distributions", *IEEE Trans. on Signal Processing*, Vol. 47, No. 2, pp. 493-504 (1999).
- [7] K. Horiuchi "Sampling Principle for Continuous Signals with Time-Varying Bands." *Information and Control*, Vol. 13, pp. 53-61, 1968.
- [8] A. Papoulis, "Error Analysis in Sampling Theory," *Proc. IEEE*, vol. 54, pp. 947-955, 1966.
- [9] N. Peterfreund and Y. Y. Zeevi, "Nonuniform Image Representation in Area-of-Interest Systems", *IEEE Trans. on Image Processing*, Vol. 4, No. 9, pp. 1202-1212, 1995.
- [10] M. A. Poletti "The Development of Instantaneous Bandwidth via Local Signal Expansion," *Signal Processing*, Vol. 31, No. 3, pp. 273-281, 1993.
- [11] M. Porat and G. Shachor, "Signal Representation in the combined Phase - Spatial space: Reconstruction and Criteria for Uniqueness", *IEEE Trans. on Signal Processing*, Vol. 47, No. 6, pp. 1701-1707 , 1999.
- [12] M. Porat and Y. Y. Zeevi, "The Generalized Gabor Scheme of Image Representation in Biological and Machine Vision," *IEEE Trans. Patt. Anal. and Machine Intell.*, Vol. PAMI-10, No. 4, pp. 452-468, 1988.
- [13] W. Rieck, "SAR Imaging of Moving Targets: Application of Time-Frequency Distribution for

- Single- and Multichannel Data”, EUROSAR’96, Koenigswinter, Germany, 1996.
- [14] A. W. Rihaczek, “Signal Energy Distribution in Time and Frequency,” *IEEE Transactions on Information Theory*, Vol. IT-14, No.3, pp. 369-374, 1968.
- [15] A. W. Rihaczek, “Principles of High Resolution Radar,” *McGraw-Hill, Inc.*, 1969.
- [16] M. Sanghadasa, P. S. Erbach and C. C. Sung, “Wavelet transform applied to synthetic aperture radar - optical implementation and adaptive techniques,” *Optical Engineering*, Vol. 33, No. 7, 2282-2288, 1994.
- [17] S. Urieli, M. Porat and N. Cohen, "Optimal Reconstruction of Images from Localized Phase", *IEEE Trans. on Image Processing*, Vol. 7, No. 6, pp. 838-853, 1998.
- [18] Y. Y. Zeevi and E. Shlomot, “Non-uniform Sampling and Anti-Aliasing in Image Representation”, *IEEE Trans. on Signal Processing*, Vol. 41, pp. 1223-1236, 1993.